

Impacts of dineutrons on nuclear compositions and neutrino reactions of the core-collapse supernova

Tatsuya Matsuki

Department of Physics, Tokyo University of Science, Tokyo 162-8601, Japan

Shun Furusawa

College of Science and Engineering, Kanto Gakuin University, Kanagawa, Japan and Interdisciplinary Theoretical and Mathematical Sciences Program (iTHEMS), RIKEN, Wako, Saitama 351-0198, Japan

Katsuhiko Suzuki

Department of Physics, Tokyo University of Science, Tokyo 162-8601, Japan

We study the nuclear compositions and neutrino reaction rates in the central region of the core-collapse supernova, assuming the existence of dineutrons (2n) and tetra-neutrons (4n). At 100 ms after core bounce, 2n and 4n are more abundant than deuterons within radii of approximately 100 km and 50 km, respectively. Compared to the model ignoring the existence of 2n and 4n , the mass fraction of neutrons up to a radius of 100 km reduces. Hence, the neutrino absorption and antineutrino emission rates decrease by approximately 40%–50%. Conversely, those of protons, deuterons, and ${}^4\text{He}$ increase, leading to the increase in the neutrino emission and antineutrino absorption rates by approximately eight times within a radius of 100 km.

I. INTRODUCTION

Core-collapse supernovae are phenomena that occur when a massive star with mass $\gtrsim 10 M_\odot$ dies. Several simulations have shown that the shock wave generated in core bounce is delayed and halted by energy loss due to iron decomposition reactions and neutrino emissions. Multidimensional effects such as convection improve the efficiency of this neutrino heating mechanism; moreover, the explosion has been reproduced by these effects in multidimensional simulations [1].

After core bounce and shock propagation, the central region within the shock radius is a hot and dense environment with an excess of neutrons. Light elements such as deuterons and ${}^4\text{He}$ are abundant in the central region at subsaturation densities [2]. In almost all simulations, detailed reactions between light elements and neutrinos are not considered; however, the weak interactions may affect neutrino emissions and the shock revival [3–5].

Meanwhile, the existence of multineutron states is under debate [6, 7]. Dineutrons (2n) were theoretically predicted in neutron halo [8], and some experiments involving neutron-rich nuclei have supported their existence [9, 10]. The dineutron is known to be unbound, and its binding energy is believed to be approximately -100 keV in free space, which is consistent with a negative neutron-neutron scattering length [11, 12]. Furthermore, tetra-neutrons (4n) have been indirectly observed as both a possible resonant state and a weakly bound state [13–16].

The impact of multineutrons on astrophysics has been a topic of discussion; for example, the role of 2n in nucleosynthesis during the early universe [17, 18] and the potential influence of 4n on the structure of neutron stars [19]. Additionally, Panov et al. [20] investigated the role of 2n and 4n in high-temperature and subsatura-

tion density environments such as supernova matter and found that 2n is present near the central region nearly as much as other light elements such as deuterons. However, the calculation is based on a spherically symmetric supernova simulation, and their impacts on neutrino reactions are not discussed.

In this paper, we focus on the roles of 2n and 4n in the supernova. Using the results of the supernova simulation with the axial symmetry approximation [21] to characterize the thermodynamic environment, and assuming the existence of 2n and 4n , we calculate the nuclear compositions at 100 ms after core bounce. We apply the nuclear statistical equilibrium approximation to determine the nuclear compositions, which works well for describing the central region of core-collapse supernovae. Subsequently, we use our model to calculate the neutrino reaction with the supernova matter, which may impact on the supernova dynamics [22–24]. We will discuss in detail the roles of the multineutron states in neutrino reactions.

This paper is organized as follows. Section II describes the models used to calculate the nuclear compositions and neutrino reaction rates. Section III presents the results and Section IV gives a summary and discussion of the study.

II. MODEL

We use the natural unit with $\hbar = 1, c = 1$ and calculate the nuclear compositions of the supernova matter. The mass density ρ_B , electron ratio Y_e , and temperature T are obtained from the recent supernova simulation through axial symmetry approximation [21]. Because the temperature is higher than 0.4 MeV, we assume that the nucleons and nuclei are in nuclear statistical equilibrium (NSE), in which the chemical potential of a nucleus with

neutron number N and proton number Z is given by

$$\mu_{N,Z} = N\mu_N + Z\mu_Z \quad (1)$$

Moreover, we assume that the nucleons and nuclei behave as the ideal Boltzmann gases, and their number densities $n_{N,Z}$ are calculated as

$$n_{N,Z} = \kappa g_{N,Z} \left(\frac{M_{N,Z} k_B T}{2\pi} \right)^{3/2} \exp \left(\frac{\mu_{N,Z} - M_{N,Z}}{k_B T} \right) \quad (2)$$

where $g_{N,Z}$ is internal degrees of freedom and κ is the factor of the excluded volume effect: $\kappa = 1$ for nucleons and $\kappa = 1 - n_B/n_0$ for nuclei with the baryon number density n_B and nuclear saturation density n_0 [2].

The mass of nucleus $M_{N,Z} = Nm_N + Zm_p - B_{N,Z}$ is calculated in terms of the binding energy $B_{N,Z}$ obtained from experiments done on the Earth; 3556 nuclei considered [25]. As for 2n and 4n , we follow previous works and adopt $B_{2n} = -0.066$ MeV [20] and 0.42 MeV [16] as the binding energies of 2n and 4n , respectively. To determine the nuclear compositions, we solve the following two equations for nucleons and nuclei

$$\sum_{N,Z} n_{N,Z}(N+Z) = n_B, \quad (3)$$

$$\sum_{N,Z} n_{N,Z}Z = Y_e n_B. \quad (4)$$

Equations (3) and (4) express the local baryon number conservation and the local charge conservation, respectively.

We now proceed to calculate the neutrino scattering processes with the supernova matter mediated by the weak interaction. While both charged and neutral current interactions contribute to neutrino emissivity [23], we focus solely on the charged current interaction, for simplicity, aiming to clarify the role of 2n under the supernova environment. The weak Hamiltonian for the charged current interaction is expressed in terms of the hadron current J_λ and the lepton current L_λ ;

$$H_W = \frac{G_F V_{ud}}{\sqrt{2}} \int d^3x [J_\lambda L^\lambda + \text{h.c.}], \quad (5)$$

$$J_\lambda = \bar{\psi}_n \gamma_\lambda (1 - a\gamma^5) \psi_p, \quad (6)$$

$$L^\lambda = \bar{\psi}_{\nu_e} \gamma^\lambda (1 - \gamma^5) \psi_e, \quad (7)$$

where $G_F = 1.1803 \times 10^{-5}$ GeV $^{-2}$ and $V_{ud} = 0.9740$ are the weak coupling constant and the Cabibbo–Kobayashi–Maskawa matrix element, respectively [23], ψ is the fermion field operator, the subscript denotes the type of particles, and $a = 1.26$ is the nucleon axial-vector coupling constant.

(i) $\nu_e + n \rightarrow e^- + p$	(vi) $e^- + p \rightarrow \nu_e + n$
(ii) $\nu_e + d \rightarrow e^- + p + p$	(vii) $e^- + d \rightarrow \nu_e + n + n$
(iii) $\nu_e + {}^2n \rightarrow e^- + n + p$	(viii) $e^+ + n \rightarrow \bar{\nu}_e + p$
(iv) $\bar{\nu}_e + p \rightarrow e^+ + n$	(ix) $e^+ + d \rightarrow \bar{\nu}_e + p + p$
(v) $\bar{\nu}_e + d \rightarrow e^+ + n + n$	(x) $e^+ + {}^2n \rightarrow \bar{\nu}_e + p + n$

TABLE I. Weak interactions.

In Table I, we list the weak interactions considered in this study. These involve possible bound (d) and quasi-bound (2n) states in the initial state, while the final states are described exclusively by free particles. We neglect d and 2n in the final state, as well as the contribution from the final state interaction and the pion exchange current, for simplicity. Since the nucleon mass is larger than lepton energies, nucleons and nuclei represented by b are treated as static in order to calculate the weak transition amplitudes [26], and nucleon energies are replaced with their chemical potentials μ_b determined from NSE calculation. For d and 2n , their energies should be calculated by solving the two-body bound state equation. Under our static approximation, however, their energies are assumed to be replaced by their chemical potentials, shifted by their binding energies as $\mu_b - B_{N,Z}$. On the other hand, the chemical potentials of the electron and neutrino are obtained from the supernova simulation [21]. The degeneracy of the lepton l is taken into account with the Fermi–Dirac distribution f^l . We then calculate the neutrino reaction rates as

$$Q = G_F^2 (1 + 3a^2) n_i^b \int \frac{d^3 p_f^l}{(2\pi)^3} \int \frac{d^3 p_i^l}{(2\pi)^3} \epsilon_\nu f_i^l (1 - f_f^l) \times 2\pi \delta(E_f^l + \sum_f \mu_f^b - E_i^l - \mu_i^b + B_{N,Z}), \quad (8)$$

where i and f represent the initial and final states, p^l and E^l are the momentum and energy of leptons, $\epsilon_\nu = E_f^l$ or E_i^l . We note that the Pauli-blocking for the final state lepton is incorporated in Eq. (8).

III. RESULTS

We first show the distributions of the density, temperature, and electron ratio obtained by the supernova simulation through the axial symmetry approximation at 100 ms and 200 ms after core bounce [21] in Figs. 1, 2, and 3, respectively. The central region exhibits higher temperature and density, and neutron-rich compared to the outer regions.

Using the thermodynamical inputs ρ_B , T and Y_e , we calculate the mass fractions $X_{N,Z} = n_{N,Z}(N+Z)/n_B$ of all nuclei including 2n and 4n . We show a two-dimensional map of the mass fractions of 2n and

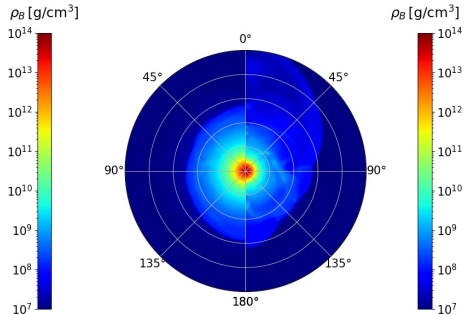


FIG. 1. Mass density distributions at 100 ms and 200 ms after core bounce on the left and right, respectively. The radius is shown up to 500 km, with scale intervals of 100 km.

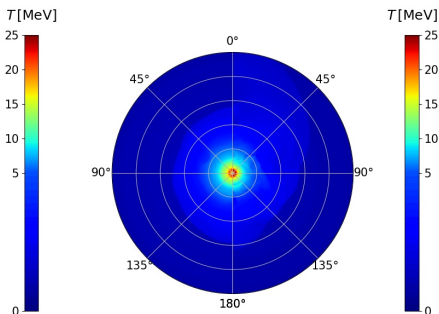


FIG. 2. Temperature distributions at 100 ms and 200 ms after core bounce on the left and right, respectively.

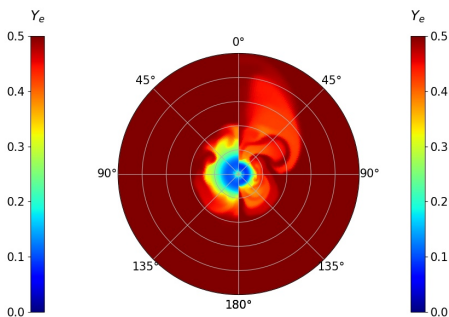


FIG. 3. Electron ratio distributions at 100 ms and 200 ms after core bounce on the left and right, respectively.

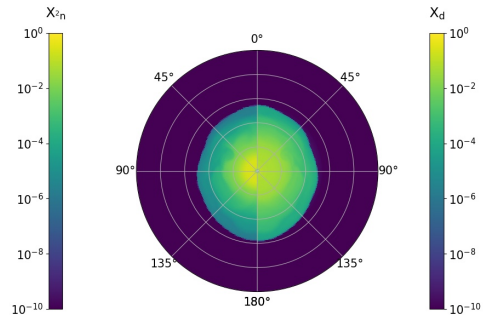


FIG. 4. Mass fraction of the dineutron (left) to the deuteron (right) at 100 ms after core bounce.

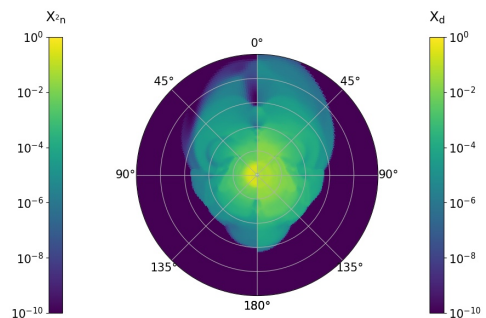


FIG. 5. Mass fraction of the dineutron (left) to the deuteron (right) at 200 ms after core bounce.

deuterons at 100 ms and 200 ms in Figs. 4 and 5, respectively. Notably, X_{2n} becomes larger than X_d inside the shock radius, although X_d has considered to be the largest around proto-neutron stars [2]. In the following, we focus on the mass fractions of the 180° angle at 100 ms, which is illustrated in Fig. 6. In this case, X_{4n} is large within a radius of approximately 50 km.

Moreover, we add the results for the nuclear composition excluding 2n and 4n in Fig. 6 by dotted curves. A significant difference is found within a radius of 100 km. The mass fraction of neutrons decreases due to populations of 2n and 4n . Interestingly, the number of the protons, deuterons, and ${}^4\text{He}$ is found to increase if we include 2n and 4n .

The isotopes of hydrogen and helium are shown in Figs. 7 and 8, respectively. The nuclei of ${}^3\text{He}$ and ${}^5\text{He}$ increase in some regions, whereas neutron-rich nuclei such as H^5 tend to decrease. The decrease of neutrons results in the decrease of the chemical potential of the neutrons. Consequently, the number of neutron-rich nuclei

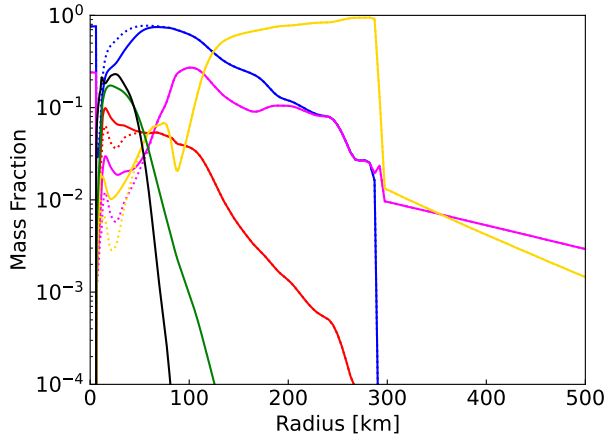


FIG. 6. Nuclear composition on the 180° angle at 100 ms after core bounce. Neutron (blue), proton (magenta), deuteron (red), ${}^4\text{He}$ (gold), 2n (green), and 4n (black) are displayed. The solid line shows the nuclear composition when the presence of 2n and 4n is considered, and the dotted line shows one when they are not.

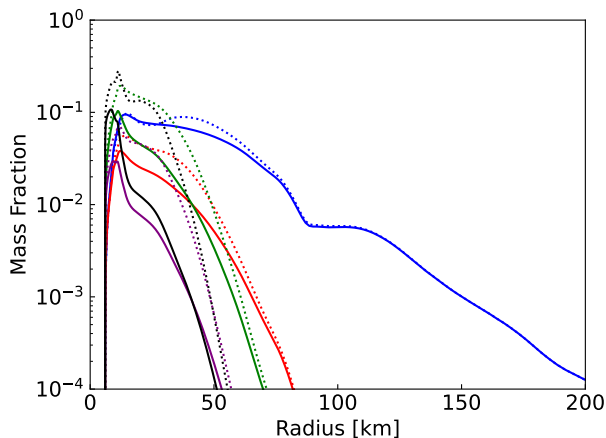


FIG. 7. The isotopes of hydrogen within the region up to 200 km. ${}^3\text{H}$ (blue), ${}^4\text{H}$ (red), ${}^5\text{H}$ (green), ${}^6\text{H}$ (purple), and ${}^7\text{H}$ (black) are displayed.

decreases, leading to an increase in the number of protons, deuterons, and ${}^4\text{He}$ through the total proton conservation of Eq. 4.

For completeness, we calculated the nuclear composition for different values of the binding energy of 2n , and the results are presented in Fig. 9. As shown in previous studies [20], the binding energy of 2n affects its mass fraction; the maximum mass fraction of 2n with $B_{2n} = 1.0$ MeV is approximately double that of the model with $B_{2n} = -3.0$ MeV.

We finally calculated the neutrino and antineutrino reaction rates of the model with $B_{2n} = -0.066$ MeV within a radius of 100 km, where the impact of 2n on the nu-

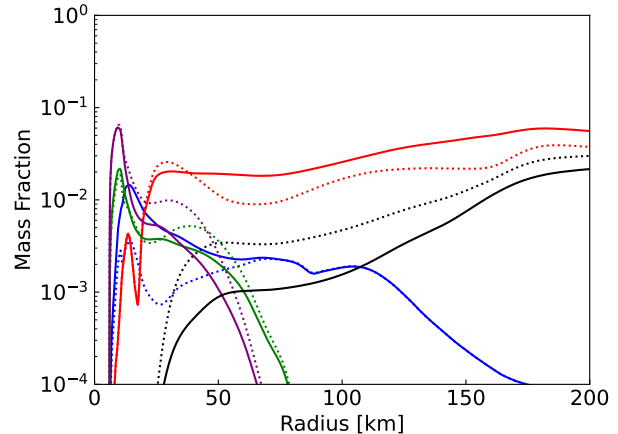


FIG. 8. The isotopes of helium within the region up to 200 km. ${}^3\text{He}$ (blue), ${}^5\text{He}$ (red), ${}^6\text{He}$ (green), ${}^7\text{He}$ (purple), and ${}^8\text{He}$ (black) are displayed.

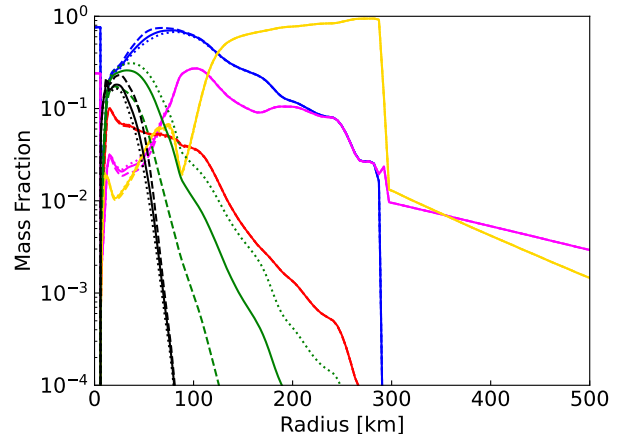


FIG. 9. The nuclear compositions for different values of the binding energy of 2n . The solid, dashed, and dotted lines represent the nuclear compositions at -0.066 MeV, -3.0 MeV, and 1.0 MeV, respectively. The colors in the graph have the same meaning as in Fig. 6.

clear compositions is significant. We show in the Fig. 10 the results for the electron-type neutrino absorption rates (i)-(iii) and antineutrino emission rates (viii)-(x), which are reactions involving neutrons, deuterons, and 2n . We also calculated the ratio of the reaction rates in the presence of 2n and 4n to those without them. The neutrino absorption and antineutrino emission rates decrease by approximately 40%–50% due to the decrease in neutrons. In Fig. 11 we show the results for the neutrino emission rates (vi) and (vii), and antineutrino absorption rates (iv) and (v), which are reactions involving protons and deuterons. Since the number of protons and deuterons increases, the neutrino emission and antineutrino absorption rates are considered to have increased

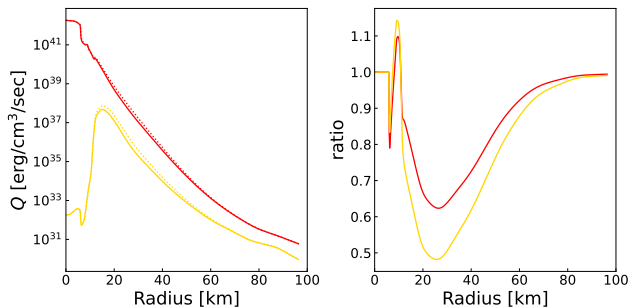


FIG. 10. Neutrino reaction rates involving the neutrino absorption (red) and antineutrino emission (gold) rates of neutrons, deuterons, and 2n .

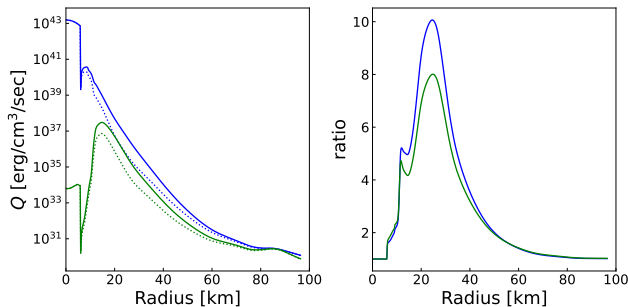


FIG. 11. Neutrino reaction rates involving neutrino emission (blue) and antineutrino absorption (green) rates of protons and deuterons.

by approximately eight times. The change in the nuclear composition has a significant effect on the electron-type neutrino reactions. The presence of 2n and 4n suppresses the reaction in which neutrons are converted to protons. Conversely, it promotes the reactions in the conversion process from protons to neutrons. This means that the existence of 2n and 4n may accelerate the neutronization of the proto-neutron star and shorten its neutrino cooling time.

IV. SUMMARY AND DISCUSSION

We have calculated the nuclear compositions and the neutrino and antineutrino reaction rates at 100 ms after core bounce using the results of a two-dimensional simulation [21], considering the existence of 2n and 4n . Compared to the deuteron, which is reported to be abun-

dant in a previous study [2], the mass fractions of 2n and 4n are larger up to a radius of approximately 100 km and 50 km, respectively. Within a radius of about 100 km, the change in nuclear composition derived from 2n and 4n is large, where the neutrons decrease and the protons, deuterons, and ${}^4\text{He}$ increase. The chemical potential of the neutrons decreases, and consequently, the number of neutron-rich nuclei such as ${}^5\text{H}$ decreases, leading to an increase in the number of the protons, deuterons, and ${}^4\text{He}$.

We have also calculated neutrino and antineutrino reaction rates by the nucleons, deuterons, and 2n . The neutrino absorption and antineutrino emission rates decrease by approximately 40%–50%, whereas the neutrino emission and antineutrino absorption rates increase by approximately eight times. These results confirm that the presence of 2n and 4n facilitates the neutronization near the central region. The early neutronization and contraction of the proto-neutron star may increase neutrino emissions and contribute to the supernova explosion or the early birth of neutron stars.

However, this study leaves room for further improvement. First, we adopted the experimental values from the Earth for the binding energy of nuclei; however, those in high-temperature and high-density environments are unknown. The change to a bound state in the environment within the supernova should be clarified and reflected in the calculations. Additionally, the binding energies of 2n and 4n have not been determined experimentally. Second, we assumed that the nucleons and nuclei are Boltzmann gases; however, the significant change in the nuclear compositions is near the central region of the proto-neutron star, which is near the subsaturation density. Since the effect of the nuclear forces cannot be ignored, the dependence on the equation of state should be investigated. Finally, the present calculation of neutrino reaction rate does not completely consider the quasisubbound states in the two-nucleon system or the energy dependence of the baryons. The application of these improvements may change the results by a few factors.

V. ACKNOWLEDGMENTS

We thank K. Mameda and K. Sumiyoshi for productive discussions, H. Nagakura for providing the simulation data, and T. Uemura for providing the nuclear statistical equilibrium code. S.F. is supported by Grant-in-Aid for Scientific Research (19K14723 and 24K00632).

[1] S. Yamada, H. Nagakura, R. Akaho, A. Harada, S. Furusawa, W. Iwakami, H. Okawa, H. Matsufuru, and K. Sumiyoshi, Physical mechanism of core-collapse supernovae that neutrinos drive, *Proceedings of the Japan Academy, Series B* **100**, 190 (2024).

[2] S. Furusawa and H. Nagakura, Nuclei in core-collapse supernovae engine, *Prog. Part. Nucl. Phys.* **129**, 104018 (2023), [arXiv:2211.01050](https://arxiv.org/abs/2211.01050) [nucl-th].

[3] N. Ohnishi, K. Kotake, and S. Yamada, Inelastic Neutrino-Helium Scatterings and Standing Accretion

- Shock Instability in Core-Collapse Supernovae, *Astrophys. J.* **667**, 375 (2007), [arXiv:astro-ph/0606187](#).
- [4] S. Furusawa, H. Nagakura, K. Sumiyoshi, and S. Yamada, The influence of inelastic neutrino reactions with light nuclei on the standing accretion shock instability in core-collapse supernovae, *Astrophys. J.* **774**, 78 (2013), [arXiv:1305.1510 \[astro-ph.HE\]](#).
- [5] T. Fischer, S. Typel, G. Röpke, N.-U. F. Bastian, and G. Martínez-Pinedo, Medium modifications for light and heavy nuclear clusters in simulations of core collapse supernovae – Impact on equation of state and weak interactions, *Phys. Rev. C* **102**, 055807 (2020), [arXiv:2008.13608 \[astro-ph.HE\]](#).
- [6] A. A. Ogloblin and Y. E. Penionzhkevich, Very neutron-rich very light nuclei, in *Treatise on Heavy Ion Science: Volume 8: Nuclei Far From Stability*, edited by D. A. Bromley (Springer US, Boston, MA, 1989) pp. 261–360.
- [7] F. M. Marqués and J. Carbonell, The quest for light multineutron systems, *Eur. Phys. J. A* **57**, 105 (2021), [arXiv:2102.10879 \[nucl-ex\]](#).
- [8] P. G. Hansen and B. Jonson, The Neutron halo of extremely neutron-rich nuclei, *EPL* **4**, 409 (1987).
- [9] K. K. Seth and B. Parker, Evidence for dineutrons in extremely neutron-rich nuclei, *Phys. Rev. Lett.* **66**, 2448 (1991).
- [10] A. Spyrou *et al.*, First Observation of Ground State Dineutron Decay: Be-16, *Phys. Rev. Lett.* **108**, 102501 (2012).
- [11] Q. Chen *et al.*, Measurement of the neutron-neutron scattering length using the pi-d capture reaction, *Phys. Rev. C* **77**, 054002 (2008).
- [12] H. W. Hammer and S. König, Constraints on a possible dineutron state from pionless EFT, *Phys. Lett. B* **736**, 208 (2014), [arXiv:1406.1359 \[nucl-th\]](#).
- [13] F. M. Marques *et al.*, The Detection of neutron clusters, *Phys. Rev. C* **65**, 044006 (2002), [arXiv:nucl-ex/0111001](#).
- [14] K. Kisamori *et al.*, Candidate Resonant Tetraneutron State Populated by the He4(He8,Be8) Reaction, *Phys. Rev. Lett.* **116**, 052501 (2016).
- [15] M. Duer *et al.*, Observation of a correlated free four-neutron system, *Nature* **606**, 678 (2022).
- [16] T. Faestermann, A. Bergmaier, R. Gernhäuser, D. Koll, and M. Mahgoub, Indications for a bound tetraneutron, *Phys. Lett. B* **824**, 136799 (2022).
- [17] J. P. Kneller and G. C. McLaughlin, The Effect of bound dineutrons upon BBN, *Phys. Rev. D* **70**, 043512 (2004), [arXiv:astro-ph/0312388](#).
- [18] J. MacDonald and D. J. Mullan, Big bang nucleosynthesis: The strong nuclear force meets the weak anthropic principle, *Phys. Rev. D* **80**, 10.1103/physrevd.80.043507 (2009).
- [19] O. Ivanytskyi, M. Ángeles Pérez-García, and C. Albertus, Tetraneutron condensation in neutron rich matter, *Eur. Phys. J. A* **55**, 184 (2019), [arXiv:1904.11512 \[nucl-th\]](#).
- [20] I. V. Panov and A. V. Yudin, Light Neutral Clusters in Supernova Matter, *Phys. Atom. Nucl.* **82**, 483 (2019), [arXiv:2003.14115 \[nucl-th\]](#).
- [21] H. Nagakura, K. Sumiyoshi, and S. Yamada, Possible early linear acceleration of proto-neutron stars via asymmetric neutrino emission in core-collapse supernovae, *Astrophys. J. Lett.* **880**, L28 (2019), [arXiv:1907.04863 \[astro-ph.HE\]](#).
- [22] T. Fischer, G. Martínez-Pinedo, M. Hempel, L. Huther, G. Röpke, S. Typel, and A. Lohs, Expected impact from weak reactions with light nuclei in core-collapse supernova simulations, *EPJ Web Conf.* **109**, 06002 (2016), [arXiv:1512.00193 \[astro-ph.HE\]](#).
- [23] S. Nasu, S. X. Nakamura, K. Sumiyoshi, T. Sato, F. Myhrer, and K. Kubodera, Neutrino Emissivities from Deuteron-Breakup and Formation in Supernovae, *Astrophys. J.* **801**, 78 (2015), [arXiv:1402.0959 \[astro-ph.HE\]](#).
- [24] S. Nakamura, T. Sato, V. P. Gudkov, and K. Kubodera, Neutrino reactions on deuteron, *Phys. Rev. C* **63**, 034617 (2001), [Erratum: *Phys. Rev. C* **73**, 049904 (2006)], [arXiv:nucl-th/0009012](#).
- [25] B. N. Laboratory, *Nudat 3.0*.
- [26] S. Reddy, M. Prakash, and J. M. Lattimer, Neutrino interactions in hot and dense matter, *Phys. Rev. D* **58**, 013009 (1998), [arXiv:astro-ph/9710115](#).